

Biomimetic Diselenide-Bridged Mesoporous Organosilica Nanoparticles as an X-ray-Responsive Biodegradable Carrier for Chemo-Immunotherapy

Dan Shao,* Fan Zhang, Fangman Chen, Xiao Zheng, Hanze Hu, Chao Yang, Zhaoxu Tu, Zheng Wang, Zhimin Chang, Junna Lu, Tianyu Li, Yuan Zhang, Li Chen, Kam W. Leong,* and Wen-fei Dong*

Chemotherapy causes off-target toxicity and is often ineffective against solid tumors. Targeted and on-demand release of chemotherapeutics remains a challenge. Here, cancer-cell-membrane-coated mesoporous organosilica nanoparticles (MONs) containing X-ray- and reactive oxygen species (ROS)-responsive diselenide bonds for controlled release of doxorubicin (DOX) at tumor sites are developed. DOX-loaded MONs coated with 4T1 breast cancer cell membranes (CM@MON@DOX) show greater accumulation at tumor sites and prolonged blood circulation time versus an uncoated control in mice bearing 4T1 orthotopic mammary tumors. Under low-dose X-ray radiation, the DOX-loaded MONs exhibit carrier degradation-controlled release via cleavage of diselenide bonds, resulting in DOX-mediated immunogenic cell death at the tumor site. Combination with a PD-L1 checkpoint blockade further enhances inhibition of tumor growth and metastasis with low systemic toxicity. Together, the findings show the promise of these biomimetic, radiation-responsive diselenide-bond-bridged MONs in chemo-immunotherapy.

chemotherapy while reducing drug doses and toxicity.^[2] The killing of tumor cells by chemotherapeutics such as anthracyclines, taxanes, mitoxantrone, and oxaliplatin elicits innate and adaptive immune responses by immunogenic cell death (ICD). In ICD, the release of tumor-associated antigens, damage-associated molecular patterns, and pro-inflammatory cytokines leads to recruitment and activation of immune effector cells such as tumor-specific T cells.^[3] This vaccine-like effect of ICD can convert an immunosuppressive tumor microenvironment (TME) to an immunogenic one that responds better to treatment with immune checkpoint blockades and adjuvants.^[4] Chemo-immunotherapy has proven effective in inhibiting the development and progression of solid tumors and distant metastases in preclinical studies and clinical

Chemotherapy is limited by off-target toxicity and ineffectiveness against solid tumors and distant metastases.^[1] Chemo-immunotherapy—the combination of chemotherapy and immunotherapy—can improve the effectiveness of

trials. However, many patients suffer from immune-related adverse events due to off-target toxicity.^[5] To reduce this toxicity and improve the therapeutic response, drug carriers have been designed to allow on-demand drug release at tumor sites.

Prof. D. Shao, F. Zhang, F. Chen, Dr. Z. Wang, Z. Chang, Prof. W.-f. Dong
CAS Key Laboratory of Bio Medical Diagnostics
Suzhou Institute of Biomedical Engineering and Technology
Chinese Academy of Sciences
Suzhou 215163, China
E-mail: wenfeidong@sibet.ac.cn


Prof. D. Shao, Dr. X. Zheng, Dr. C. Yang, Dr. Z. Tu, J. Lu, Prof. Y. Zhang
Institutes for Life Sciences
School of Biomedical Sciences and Engineering
Guangzhou International Campus
South China University of Technology
Guangzhou 510630, China
E-mail: shaodan@scut.edu.cn

Prof. D. Shao, H. Hu, Dr. C. Yang, Dr. Z. Tu, Dr. T. Li, Prof. K. W. Leong
Department of Biomedical Engineering
Columbia University
New York, NY 10027, USA
E-mail: kam.leong@columbia.edu

Prof. D. Shao, Dr. X. Zheng, Dr. C. Yang, Dr. Z. Tu, Prof. Y. Zhang
National Engineering Research Center for Tissue Restoration
and Reconstruction
South China University of Technology
Guangzhou 510630, China

Dr. X. Zheng, Prof. L. Chen
Department of Pharmacology
Nanomedicine Engineering Laboratory of Jilin Province
College of Basic Medical Sciences
Jilin University
Changchun 130021, China

Prof. K. W. Leong
Department of Systems Biology
Columbia University
New York, NY 10032, USA

 The ORCID identification number(s) for the author(s) of this article can be found under <https://doi.org/10.1002/adma.202004385>.

DOI: 10.1002/adma.202004385

Spatial, temporal, and dose control of drug release can be achieved with drug carriers that are responsive to internal stimuli such as changes in pH, redox potential, and enzymatic activity, and external stimuli such as light, radiation, temperature changes, and electric and magnetic fields.^[6] X-ray radiation is a promising external trigger due to its high penetration depth in solid tumors.^[7] Mesoporous organosilica nanoparticles (MONs) are inorganic–organic hybrid materials that are attractive for drug delivery due to their large surface area, tunable structure/chemistry, good biocompatibility, and controllable degradation.^[8] Degradation-controlled drug release from MONs has been achieved via several different degradation pathways, in response to TME stimuli such as reduced pH, increased glutathione (GSH), increased reactive oxygen species (ROS), and tumor-specific enzymes.^[8] X-ray-radiation-responsive MONs have not been previously investigated for use in degradation-controlled chemotherapeutic release.

Selenium (Se) is a nutritionally essential, multifunctional element.^[9] Diselenide bond is sensitive to X-ray radiation, and hence diselenide bond-containing polymers have been developed for X-ray-radiation-responsive drug release.^[10] Our group recently fabricated a series of diselenide-bond-bridged large-pore MONs which load and release proteins in a GSH/ROS-responsive manner.^[11] We hypothesize that these diselenide-bond-bridged MONs may serve as an effective drug carrier for X-ray-radiation-responsive drug release. We propose to construct a nanocarrier that can achieve high drug loading, immune system evasion, tumor targeting, and controlled release under low-dose radiation in the ROS-enriched tumor environment.

Here, we evaluate an X-ray-responsive diselenide-bridged MON for use in the delivery of doxorubicin (DOX) and a PD-L1 immune checkpoint blockade for chemo-immunotherapeutic treatment of solid tumors (Figure 1a). DOX is loaded into small-pore diselenide-bond-bridged MONs coated with source cancer-cell-derived membrane fragments to promote tumor targeting and immune system evasion. Low-dose X-ray radiation cleaves the diselenide bonds, promoting release of DOX, which enhances ICD at the tumor site. Combination of this treatment with a PD-L1 checkpoint blockade enhanced anti-tumor and anti-metastatic efficacy in 4T1 orthotopic mammary tumor-bearing mice *in vivo*.

Diselenide-bond-bridged MONs with a high Se density (9.9%) were prepared by a modified sol–gel method.^[11] Electron microscopy images revealed monodisperse, spherical MONs ≈ 60 nm in diameter with small pores (Figure 1b; Figure S1, Supporting Information). Fourier transform infrared and energy-dispersive X-ray spectroscopy confirmed the presence of diselenide bonds (Figure S1, Supporting Information). In solution containing 100×10^{-6} M H₂O₂ simulating ROS conditions in TME, the organosilica framework collapsed into irregular aggregates under low-dose X-ray radiation (1 Gy) within 24 h, and disassembled completely within 3 days (Figure 1c). MONs were degraded when exposed to X-ray irradiation, but they could not be further disassembled without the presence of H₂O₂ (Figure S1, Supporting Information). The mechanism of this degradation was investigated by X-ray photoelectron spectroscopy (XPS) (Figure 1d). The increase in Se 3d⁵ binding energy from 56 to 60 eV confirmed formation of seleninic acid,

indicating oxidization and cleavage of diselenide bonds. N₂ adsorption–desorption isotherms revealed type-IV isotherms (Figure 1e) that indicated a small pore size with a narrow distribution centered at 4.2 nm (Figure S1, Supporting Information). The Brunauer–Emmett–Teller surface area was 432.7 m² g⁻¹ and the total pore volume was 0.96 cm³ g⁻¹. After carboxyl modification, the small-pore MONs carrier showed high loading of DOX via electrostatic interactions (Figure S1, Supporting Information), with a passive entrapment efficiency of 25.8 wt% DOX (relative to the weight of DOX-loaded MONs). To study the X-ray responsiveness of the MONs, DOX release was characterized in 100×10^{-6} M H₂O₂-containing media (mimicking TME redox conditions) with or without low-dose X-ray radiation (Figure 1f). The MONs exhibited rapid and sustained DOX release (>70% after 96 h), but slow release (<10% after 96 h) in media lacking H₂O₂. Under 1 Gy radiation, 45.2% of loaded DOX was released in a burst-like fashion in the first 6 h; without radiation, only 18.1% of the DOX was released. Together, these results indicate the importance of both X-ray radiation and ROS in the degradative release.^[11] Compared to diselenide-bond Se polymers, our diselenide-bond-bridged MONs exhibited higher Se content, which render a better performance on low-dose X-ray-responsive drug release and treatment.

To achieve tumor-targeted and immune-evasive DOX delivery, 4T1 breast cancer cell membrane (CM) was isolated and used to coat DOX-loaded MONs (MON@DOX) as we have reported previously.^[11] CM-coated MON@DOX (CM@MON@DOX) exhibited a core–shell structure with a MON core enclosed in a thin, smooth membrane shell (Figure 2a). A slight (statistically insignificant) increase in hydrodynamic diameter was observed after adding the CM coating (Figure 2b). The surface charge decreased dramatically, to approximately that of CM vesicles (Figure 2c). To test whether the CM coating promoted colloidal stability, CM@MON@DOX and MON@DOX were dispersed in 10% fetal bovine serum-containing medium for a week. Uncoated MON@DOX showed significant aggregation; little aggregation was observed for CM@MON@DOX (Figure 2d). When FITC-labeled MONs and DiD-CM vesicles were incubated together with 4T1 breast cells for 1 h, a high degree of intracellular co-localization was observed in endosomes/lysosomes of the cells (Figure 2e), indicating cancer cell targeting by the coated MONs. Protein electrophoresis indicated the presence of 4T1 CM proteins on the CM-coated MONs (Figure S2, Supporting Information), indicating successful integration of the MONs and the CM. Source cancer cell coatings confer advantages due to the properties of the donor cells, including self-recognition and enhanced internalization by homologous cells, and immune system evasion.^[12] The ability of CM@MON@DOX to target homologous 4T1 cells was investigated by measuring the intrinsic fluorescence of DOX by flow cytometry in several cell types: 4T1 cells, MCF-10A human breast epithelial cells, and RAW264.7 macrophages (Figure 2f). CM@MON@DOX internalization was greater in 4T1 cells than in MCF-10A or RAW264.7 macrophages. The low internalization observed in macrophages might be attributed to high expression of CD47 (which promotes evasion of phagocytosis^[13]) on CM@MON@DOX (Figure S2, Supporting Information).

We next evaluated the effect of CM@MON@DOX on 4T1 cell growth *in vitro* (Figure S3, Supporting Information).

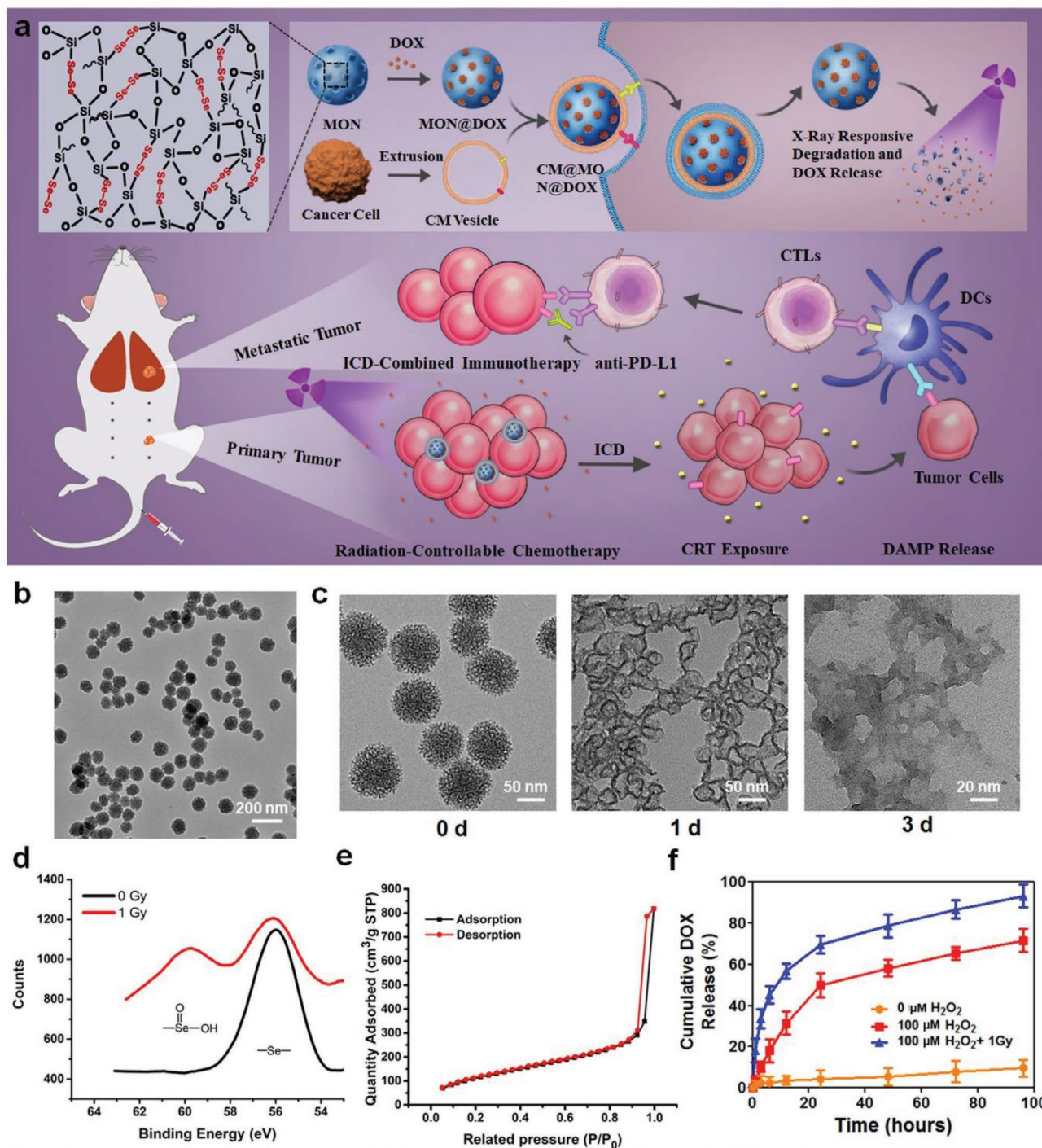


Figure 1. Preparation and characterization of mesoporous organosilica nanoparticles (MONs). a) Schematic of synthesis of diselenide-bond-bridged MONs for low-dose X-ray radiation-controllable drug release. b) TEM image of MONs (≈ 60 nm diameter). c) TEM images of MONs showing degradation at 1 d and 3 d after 1 Gy of X-ray radiation under 100×10^{-6} M H_2O_2 . d) XPS analysis of MONs before and after radiation. e) N_2 sorption isotherms of MONs. f) Drug release profiles in 100×10^{-6} M H_2O_2 with or without radiation. Data are presented as mean \pm SD ($n = 3$).

Bare MONs without DOX inhibit cancer cell growth at high MONs concentrations ($>250 \mu\text{g mL}^{-1}$) due to the anti-tumor effect of Se.^[11,14] However, MON@DOX exhibited comparable killing efficiency at much lower MONs concentrations. CM@MON@DOX inhibited 4T1 cell growth to a greater extent

than uncoated MON@DOX, indicating homologous cell targeting due to the coating. Under 1 Gy of X-ray radiation, the IC_{50} of CM@MON@DOX was 2.1-fold lower than the IC_{50} of uncoated MON@DOX (Figure 2g), again indicating the importance of the CM coating. This low dose of radiation did not

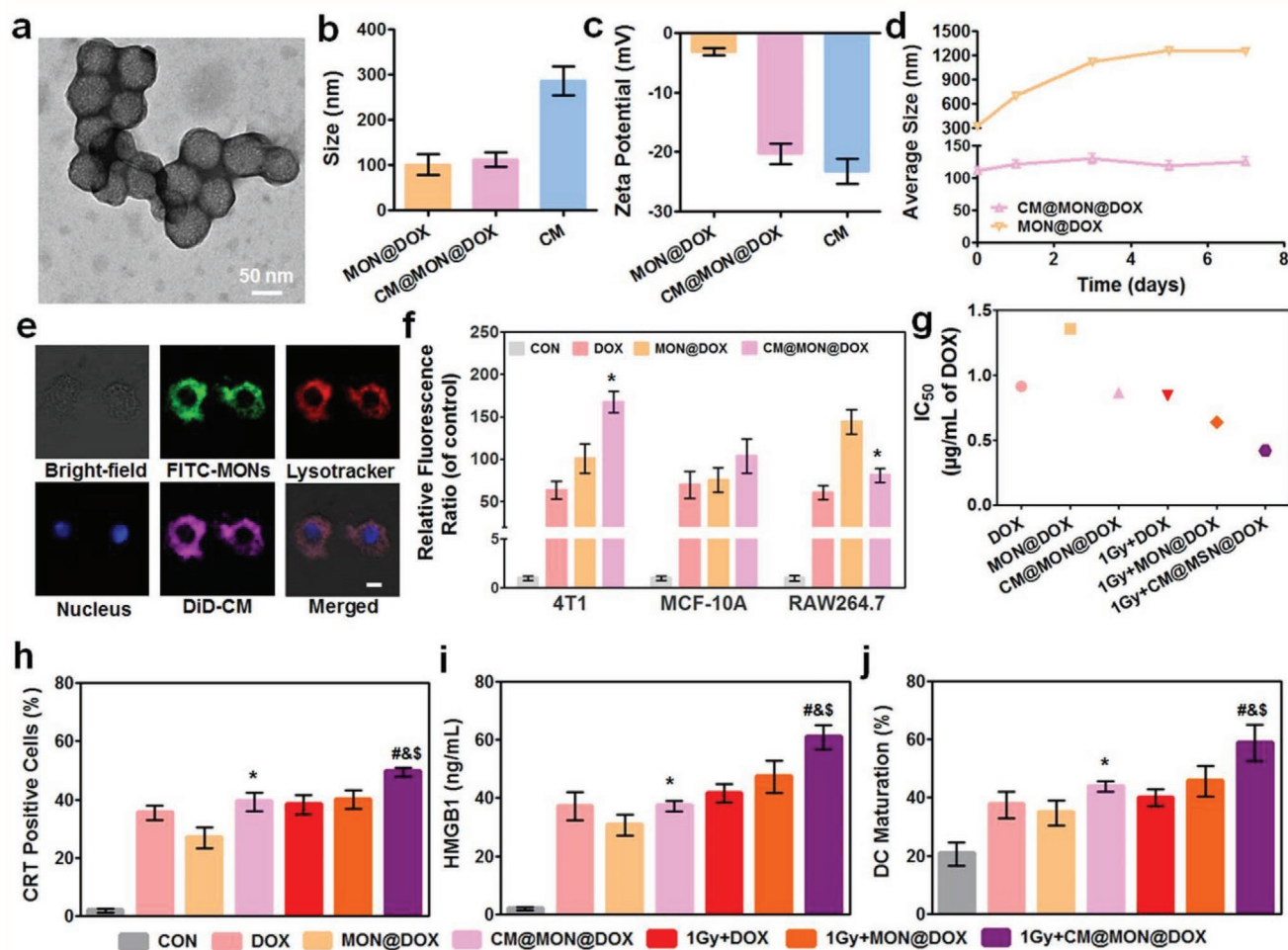


Figure 2. Characterization of cancer cell membrane-coated CM@MON@DOX in vitro. a) TEM image. b) Size of CM@MON@DOX, MON@DOX, and CM vesicles. c) Zeta potential. d) Colloidal stability of CM@MON@DOX and MON@DOX in DMEM plus 10% FBS for 7 days. e) Intracellular co-localization of DiD-labeled CM vesicles (red) and FITC-labeled MONs (green) in 4T1 cells after 1 h incubation. Scale bars: 5 µm. f) Fluorescence intensity of 4T1, MCF-10A, and RAW264.7 cells after incubation with CM@MON@DOX or MON@DOX for 6 h. All data are mean ± SD ($n = 3$). * $p < 0.05$ compared with MON@DOX group. 4T1 cells treated with CM@MON@DOX for 3 h followed by exposure to X-ray irradiation (1 Gy). g) IC₅₀ of each group after 24 h of exposure. h) Percentage of CRT-positive cells and i) amount of released HMGB1 after 24 h. j) Percentage of mature DCs (CD11c⁺CD80⁺CD86⁺) after co-incubation with 4T1 cells with different treatments for 24 h. All data are mean ± SD ($n = 3$). *, #, &, § $p < 0.05$ compared with the MON@DOX (*), 1Gy + DOX (#), 1Gy + MON@DOX (&), and 1Gy + CM@MON@DOX (§).

appear toxic to the 4T1 cells (Figure S3, Supporting Information). DOX induces ICD and release of calreticulin (CRT) and chromatin-binding protein high mobility group B1 (HMGB1), resulting in activation of antigen-presenting cells.^[15] We characterized the immunogenic phenotypes of 4T1 cells after treatment with X-ray radiation and various treatments: CM@MON@DOX and MON@DOX with and without radiation, radiation only, DOX only, and an untreated control (Figure 2h–j). Under radiation, CM@MON@DOX induced the highest percentage of CRT-positive cells (Figure 2h), the highest level of HMGB1 (Figure 2i), and the greatest DC maturation in vitro (Figure 2j), indicating that CM@MON@DOX + low-dose X-ray radiation promotes ICD and may be useful as an anti-tumor vaccine.

A challenge in chemotherapeutic delivery is achieving a long blood circulation time. We compared the pharmacokinetic profiles of DOX, MON@DOX, and CM@MON@DOX by

adma202004385 DOX concentration in mice (Figure 3a). CM@MON@DOX exhibited an elimination half-life ($T_{1/2}$, 18.4 h) that was remarkably higher than that of MON@DOX (6.6 h) and free DOX (5.7 h). This enhanced blood retention suggests that the CM coating confers invisibility to the host immune system in addition to improving colloidal stability. We examined the biodistribution of CM@MON@DOX by determining the silicon (Si) content of tumor tissue and major organs in treated mice bearing 4T1 orthotopic mammary tumors (Figure 3b). The greatest accumulation of Si at the tumor site was found in mice in the CM@MON@DOX treatment group at 12 h after intravenous injection (Figure S4, Supporting Information), indicating that 12 h post-injection might be the best timing for X-ray radiation in this model. Si accumulation at the tumor site at 12 h was significantly higher in the CM@MON@DOX group than in the MON@DOX group, indicating the importance of the cancer cell coating for tumor targeting in vivo (as observed

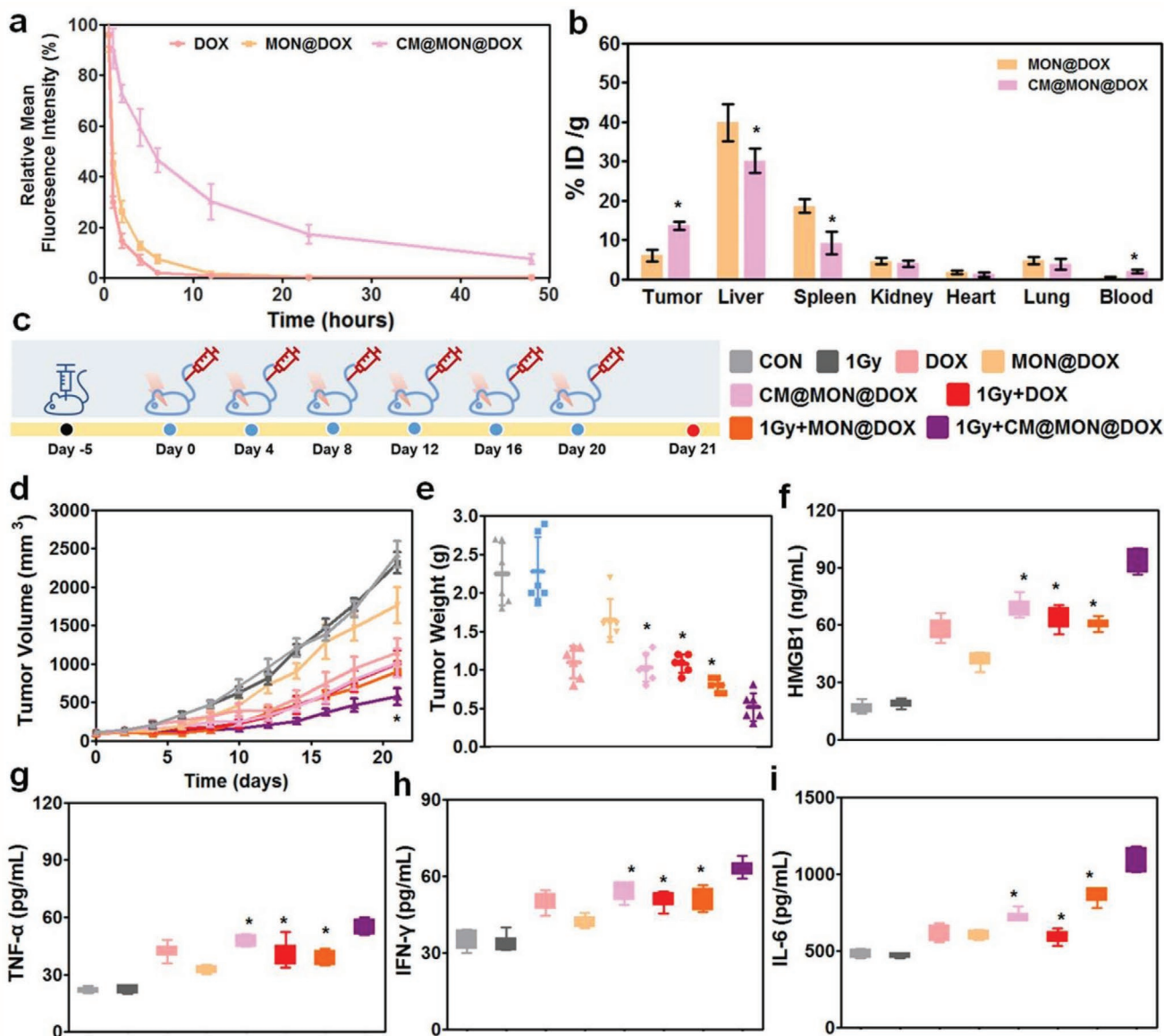


Figure 3. Low-dose (1 Gy) X-ray-radiation-responsive chemotherapy and anti-tumor immune response in mice in vivo. a) Blood circulation time and b) biodistribution of CM@MON@DOX, uncoated MON@DOX, and free DOX in 4T1-tumor-bearing mice. All data are mean \pm SD ($n = 5$). * $p < 0.05$ compared with MON@DOX. c) Schematic of treatment schedule. Mice were randomly divided into eight groups: 1) saline only, 2) 1 Gy only, 3) DOX only, 4) MON@DOX, 5) CM@MON@DOX, 6) 1 Gy + DOX, 7) 1 Gy + MON@DOX, and 8) 1 Gy + CM@MON@DOX. d) Tumor volume. Data are mean \pm SD ($n = 6$). * $p < 0.05$ compared with CM@MON@DOX, 1 Gy + DOX, and 1 Gy + MON@DOX group, respectively. e) Tumor weight, f) tumor HMGB1 level. g) TNF- α , h) IFN- γ , and i) IL-6 levels. Data are mean \pm SD ($n = 6$). * $p < 0.05$ compared with 1 Gy + CM@MON@DOX group.

in vitro). Enrichment of CM@MON@DOX in the reticuloendothelial system including liver and spleen was remarkably lower than that of uncoated MON@DOX, indicating that the CM coating promoted immune cell evasion in vivo.

Encouraged by these in vivo results, we examined the therapeutic efficacy of the X-ray-responsive CM@MON@DOX in mice bearing 4T1 orthotopic mammary tumor (Figure 3c–e; Figure S5, Supporting Information). All mice treated with DOX or DOX-based nanotherapeutics exhibited a decrease in tumor volume and tumor weight at the end of the treatment period relative to the untreated group. The CM coating significantly enhanced the anti-tumor effect and CM@MON@DOX had a

therapeutic index comparable to that of free DOX. Importantly, mice treated with low-dose X-ray radiation and CM@MON@DOX showed the greater anti-tumor effect among all groups. Low-dose X-ray radiation alone or combined with free DOX did not affect the tumor growth. To explore the anti-tumor immune response, ICD levels were evaluated by measuring levels of HMGB1 and the cytokines tumor necrosis factor- α (TNF- α), interferon- γ (IFN- γ), and interleukin-6 (IL-6). The CM@MON@DOX plus radiation group exhibited the greatest release of HMGB1 (Figure 3f), and higher serum levels of TNF- α , IFN- γ , and IL-6 than untreated control and DOX-only groups (Figure 3g–i). These results demonstrate that treatment

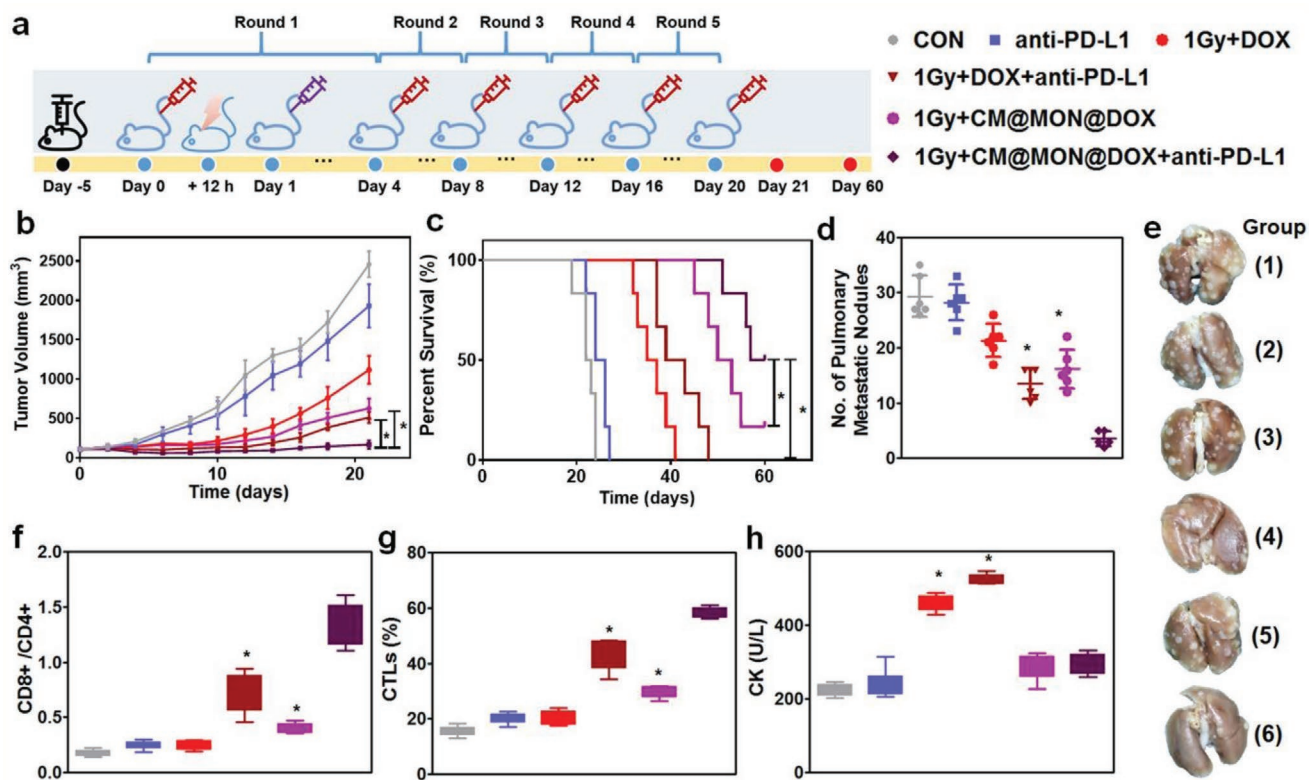


Figure 4. Radiation-responsive chemo-immunotherapy in vivo. a) Treatment schedule in a 4T1 orthotopic mammary tumor model. Mice were randomly divided into six groups: 1) saline only, 2) anti-PD-L1, 3) 1 Gy + DOX, 4) 1 Gy + DOX + anti-PD-L1, 5) 1 Gy + CM@MON@DOX, and 6) 1 Gy + CM@MON@DOX + anti-PD-L1. b) Tumor volume. c) Survival time, $n = 6$ mice per group; $*p < 0.05$, Kaplan–Meier survival analysis. d) Number of pulmonary metastatic nodules. e) Images of lung tissues with metastatic nodules from 4T1-tumor-bearing mice in each group over 21 d. f, g) At day 6 of chemoimmunotherapy, serum and primary tumor tissue were collected for analysis of ratio of CD8⁺/CD4⁺ T cells (f) and CTL content (g). h) Phosphocreatine kinase (CK) level in serum over 21 d. Data are mean \pm SD ($n = 6$). In (b) and (d–g): $*p < 0.05$ compared with 1 Gy + CM@MON@DOX + anti-PD-L1 group. In (h): $*p < 0.05$ compared with control group.

with low-dose X-ray radiation and CM@MON@DOX elicited an immune response and enhanced the inhibition of tumor growth in vivo.

We next combined this treatment with a PD-L1 immune checkpoint inhibitor and examined the systemic anti-tumor ability and anti-metastatic effect of this chemo-immunotherapeutic treatment in vivo. **Figure 4a** depicts the procedure used. The combined treatment (anti-PD-L1 + low-dose X-ray + CM@MON@DOX) exhibited greater inhibition of tumor growth and pulmonary metastasis than chemotherapy alone (without anti-PD-L1). Anti-PD-L1 alone did not delay tumor progression or metastasis (**Figure 4b–e**; **Figure S6**, Supporting Information). Intriguingly, in the chemo-immunotherapy treatment group, half of the mice became tumor free and survived to day 60 post-tumor cell challenge. Similar results were observed when comparing inhibition of pulmonary metastasis between different treatments (**Figure 4d–e**; **Figure S6**, Supporting Information). Notably, the CM@MON@DOX + radiation + anti-PD-L1 group exhibited the most pronounced anti-tumor immune response, including an increased ratio of CD8⁺ to CD4⁺ T cells (**Figure 4f**), cytotoxic T lymphocyte (CTL) infiltration (**Figure 4g**), and pro-inflammatory cytokine production (**Figure S6**, Supporting Information). These results suggest that the combination of immune checkpoint blockade and

DOX-induced ICD elicits systemic anti-tumor immunity.^[16] Together, the combined chemo-immunotherapy led to a remarkable systemic therapeutic outcome including suppression of the progression of both primary and metastatic tumors.

The in vivo safety profile of the combined chemo-immunotherapy was evaluated by mouse body weight, serum biochemistry, and hematoxylin-eosin staining (**Figures S7** and **S8**, Supporting Information). We observed a cyclical decrease in body weight in mice receiving DOX treatment with or without anti-PD-L1, and significantly increased levels of liver and kidney function enzymes including aspartate aminotransferase, alanine aminotransferase, urea nitrogen, and creatinine (**Figure S7**, Supporting Information). Importantly, the cardiovascular toxicity of DOX was indicated by an elevated level of phosphocreatine kinase (**Figure 4h**), myocardial tissue swelling, and inflammatory cell infiltration (**Figure S8**, Supporting Information), consistent with our previous study.^[17] Interestingly, the combined chemo-immunotherapy group exhibited greater cardiovascular toxicity than the chemotherapy-only group (without anti-PD-L1), suggesting that DOX contributes to adverse immune-related effects when combined with anti-PD-L1. Encouragingly, negligible pathological changes were found in terms of body weight, serum biochemical parameters, and histopathology of the liver, spleen, kidney, heart, and lung in the

CM@MON@DOX-mediated chemotherapy and chemo-immunotherapy groups, indicating limited adverse immune-related effects.

In summary, we developed a new strategy for chemo-immunotherapy in which source cancer CM-coated, diselenide-bond-bridged MONs serve as a biomimetic, X-ray/ROS-responsive drug carrier. Biodegradable diselenide-bond-bridged MONs were designed for DOX loading and delivery, and demonstrated degradation-controlled drug release by low-dose X-ray-induced cleavage of the diselenide bonds. Coating the MONs with cancer CM-derived vesicles resulted in cancer cell targeting and immune system evasion. This chemo-immunotherapy boosts DOX-induced ICD and elicits systemic anti-tumor immunity which eradicates primary and metastatic tumors while minimizing off-target adverse effects. These biomimetic, radiation-responsive diselenide-bond-bridged MONs have the potential to achieve efficient and safe chemo-immunotherapy effects in the clinic. The presented work suggests a design of radiation-responsive carrier for the controlled delivery of therapeutic agents, such as active pharmaceutical ingredients, nucleic acids, and proteins, with a possibility of on-demand release and low systemic toxicity.

Supporting Information

Supporting Information is available from the Wiley Online Library or from the author.

Acknowledgements

D.S., F.Z., and F.C. contributed equally to this work. Prof. Wen Sun, Prof. Mingqiang Li, Dr. Jianati Dawulieti, Dr. Xue Zhang, Ya-wei Zhao, Yue Zhang, Huize Yan, Xing Meng, and Xiaochun Xie are acknowledged for their help in preparing the paper. This work was supported by the National Natural Science Foundation of China (Grant Nos. 81902166, 81771982, 81601609, 61535010, and 8160071152), the National Key R&D Program of China (Grand Nos. 2017YFF0108600 and 2017YFC0211900), the Natural Science Foundation of Jiangsu Province (Nos. BK20181236 and BE2019683), and the Science and Technology Department of Jinan City (2018GXRC016). All animal experimental protocols, including obtaining the mouse bone marrow dendritic cells (BMDCs) from the bone marrow of C57BL/6 mice, were approved by the Ethics Committee for the Use of Experimental Animals of Jilin University. 4T1 murine cancer cell line (4T1), MCF-10A human mammary epithelial cell line, RAW264.7 murine macrophages cell line (RAW264.7) were obtained from American Type Culture Collection (ATCC, Manassas, VA, USA).

Conflict of Interest

The authors declare no conflict of interest.

Keywords

biodegradable mesoporous organosilica nanoparticles, biomimetic, chemo-immunotherapy, diselenide bonds, X-ray radiation responsivity

Received: June 28, 2020

Revised: August 26, 2020

Published online: November 9, 2020

- [1] a) V. T. DeVita, E. Chu, *Cancer Res.* **2008**, *68*, 8643; b) K. Nurgali, R. T. Jagoe, R. Abalo, *Front. Pharmacol.* **2018**, *9*, 245; c) G. S. Karagiannis, J. S. Condeelis, M. H. Oktay, *Clin. Exp. Metastasis* **2018**, *35*, 269.
- [2] a) A. M. Cook, W. J. Lesterhuis, A. K. Nowak, R. A. Lake, *Curr. Opin. Immunol.* **2016**, *39*, 23; b) R. A. Lake, B. W. Robinson, *Nat. Rev. Cancer* **2005**, *5*, 397.
- [3] a) D. V. Krysko, A. D. Garg, A. Kaczmarek, O. Krysko, P. Agostinis, P. Vandenabeele, *Nat. Rev. Cancer* **2012**, *12*, 860; b) O. Kepp, L. Galluzzi, I. Martins, F. Schlemmer, S. Adjemian, M. Michaud, A. Q. Sukkurwala, L. Menger, L. Zitvogel, G. Kroemer, *Cancer Metastasis Rev.* **2011**, *30*, 61.
- [4] a) L. Galluzzi, A. Buqué, O. Kepp, L. Zitvogel, G. Kroemer, *Nat. Rev. Immunol.* **2017**, *17*, 97; b) O. Kepp, L. Zitvogel, G. Kroemer, *Oncolimmunology* **2019**, *8*, 1606665; c) C. Pfirschke, C. Engblom, S. Rickelt, V. Cortez-Retamozo, C. Garris, F. Pucci, T. Yamazaki, V. Poirier-Colame, A. Newton, Y. Redouane, *Immunity* **2016**, *44*, 343.
- [5] a) P. Schmid, S. Adams, H. S. Rugo, A. Schneeweiss, C. H. Barrios, H. Iwata, V. Diéras, R. Hegg, S.-A. Im, G. S. Wright, *N. Engl. J. Med.* **2018**, *379*, 2108; b) L. Gandhi, D. Rodríguez-Abreu, S. Gadgeel, E. Esteban, E. Felip, F. De Angelis, M. Domine, P. Clingan, M. J. Hochmair, S. F. Powell, *N. Engl. J. Med.* **2018**, *378*, 2078.
- [6] a) P. Davoodi, L. Y. Lee, Q. Xu, V. Sunil, Y. Sun, S. Soh, C.-H. Wang, *Adv. Drug Delivery Rev.* **2018**, *132*, 104; b) X. Li, J. Kim, J. Yoon, X. Chen, *Adv. Mater.* **2017**, *29*, 1606857; c) F. Gong, N. Yang, X. Wang, Q. Zhao, Q. Chen, Z. Liu, L. Cheng, *Nano Today* **2020**, *32*, 100851.
- [7] a) X. Chen, J. Song, X. Chen, H. Yang, *Chem. Soc. Rev.* **2019**, *48*, 3073; b) W. Deng, W. Chen, S. Clement, A. Guller, Z. Zhao, A. Engel, E. M. Goldys, *Nat. Commun.* **2018**, *9*, 2713; c) K. Lu, C. He, N. Guo, C. Chan, K. Ni, G. Lan, H. Tang, C. Pelizzari, Y.-X. Fu, M. T. Spiotto, *Nat. Biomed. Eng.* **2018**, *2*, 600.
- [8] a) Y. Chen, J. Shi, *Adv. Mater.* **2016**, *28*, 3235; b) X. Du, X. Li, L. Xiong, X. Zhang, F. Kleitz, S. Z. Qiao, *Biomaterials* **2016**, *91*, 90; c) X. Du, F. Kleitz, X. Li, H. Huang, X. Zhang, S. Z. Qiao, *Adv. Funct. Mater.* **2018**, *28*, 1707325; d) Z. Teng, W. Li, Y. Tang, A. Elzatahry, G. Lu, D. Zhao, *Adv. Mater.* **2019**, *31*, 1707612; e) B. Yang, Y. Chen, J. Shi, *Mater. Sci. Eng. R Rep.* **2019**, *137*, 66; f) J. Dawulieti, M. Sun, Y. Zhao, D. Shao, H. Yan, Y. Lao, H. Hu, L. Cui, X. Lv, F. Liu, C. Chi, Y. Zhang, M. Li, M. Zhang, H. Tian, X. Chen, K. Leong, L. Chen, *Sci. Adv.* **2020**, *6*, eaay7148.
- [9] a) M. P. Rayman, *Lancet* **2012**, *379*, 1256; b) M. Vinceti, T. Filippini, C. Del Giovane, G. Dennert, M. Zwahlen, M. Brinkman, M. P. Zeegers, M. Horneber, R. D'Amico, C. M. Crespi, *Cochrane Database Syst. Rev.* **2018**, *1*, CD005195; c) Y. Hu, T. Liu, J. Li, F. Mai, J. Li, Y. Chen, Y. Jing, X. Dong, L. Lin, J. He, *Biomaterials* **2019**, *222*, 119397.
- [10] a) W. Cao, L. Wang, H. Xu, *Nano Today* **2015**, *10*, 717; b) T. Li, S. Pan, S. Gao, W. Xiang, C. Sun, W. Cao, H. Xu, *Angew. Chem., Int. Ed.* **2020**, *132*, 2722; c) S. Gao, T. Li, Y. Guo, C. Sun, B. Xianyu, H. Xu, *Adv. Mater.* **2020**, *32*, 1907568.
- [11] D. Shao, M. Li, Z. Wang, X. Zheng, Y. H. Lao, Z. Chang, F. Zhang, M. Lu, J. Yue, H. Hu, *Adv. Mater.* **2018**, *30*, 1801198.
- [12] a) R. H. Fang, A. V. Kroll, W. Gao, L. Zhang, *Adv. Mater.* **2018**, *30*, 1706759; b) H. Yan, D. Shao, Y. H. Lao, M. Li, H. Hu, K. W. Leong, *Adv. Sci.* **2019**, *6*, 1900605; c) L. Rao, B. Cai, L.-L. Bu, Q.-Q. Liao, S.-S. Guo, X.-Z. Zhao, W.-F. Dong, W. Liu, *ACS Nano* **2017**, *11*, 3496.
- [13] a) E. Koh, E. J. Lee, G.-H. Nam, Y. Hong, E. Cho, Y. Yang, I.-S. Kim, *Biomaterials* **2017**, *121*, 121; b) H. Sun, J. Su, Q. Meng, Q. Yin, L. Chen, W. Gu, P. Zhang, Z. Zhang, H. Yu, S. Wang, *Adv. Mater.* **2016**, *28*, 9581; c) A. Pasto, F. Giordano, M. Evangelopoulos, A. Amadori, E. Tasciotti, *Clin. Transl. Med.* **2019**, *8*, 1.

- [14] a) Y. Huang, L. He, W. Liu, C. Fan, W. Zheng, Y. Wong, T. Chen, *Biomaterials* **2013**, *34*, 7106; b) T. Li, H. Xu, *Cell Rep. Phys. Sci.* **2020**, *1*, 100111.
- [15] a) J. Lu, X. Liu, Y.-P. Liao, F. Salazar, B. Sun, W. Jiang, C. H. Chang, J. Jiang, X. Wang, A. M. Wu, *Nat. Commun.* **2017**, *8*, 1811; b) S. Bai, L. L. Yang, Y. Wang, T. Zhang, L. Fu, S. Yang, S. Wan, S. Wang, D. Jia, B. Li, *Small* **2020**, *16*, 2000214; c) E. M. Mastria, L. Y. Cai, M. J. Kan, X. Li, J. L. Schaal, S. Fiering, M. D. Gunn, M. W. Dewhirst, S. K. Nair, A. Chilkoti, *J. Controlled Release* **2018**, *269*, 364.
- [16] a) X. Duan, C. Chan, W. Lin, *Angew. Chem., Int. Ed.* **2019**, *58*, 670; b) G. Yang, L. Xu, Y. Chao, J. Xu, X. Sun, Y. Wu, R. Peng, Z. Liu, *Nat. Commun.* **2017**, *8*, 1; c) S. Ruan, R. Xie, L. Qin, M. Yu, W. Xiao, C. Hu, W. Yu, Z. Qian, L. Ouyang, Q. He, *Nano Lett.* **2019**, *19*, 8318; d) Z. Wang, F. Zhang, D. Shao, Z. Chang, L. Wang, H. Hu, X. Zheng, X. Li, F. Chen, Z. Tu, *Adv. Sci.* **2019**, *6*, 1901690.
- [17] a) F. Zhang, Y. Jia, X. Zheng, D. Shao, Y. Zhao, Z. Wang, J. Dawulieti, W. Liu, M. Sun, W. Sun, *Acta Biomater.* **2019**, *100*, 352; b) D. Shao, J. Li, X. Zheng, Y. Pan, Z. Wang, M. Zhang, Q.-X. Chen, W.-F. Dong, L. Chen, *Biomaterials* **2016**, *100*, 118; c) Z. Wang, D. Shao, Z. Chang, M. Lu, Y. Wang, J. Yue, D. Yang, M. Li, Q. Xu, W.-f. Dong, *ACS Nano* **2017**, *11*, 12732.